water

MDPI

Article

Flood Simulation and Flood Risk Reduction Strategy in Irrigated Areas

Zhenyang Liu [1,2], Yujiang Xiong [3] and Junzeng Xu [1,2,*]

[1] State Key Laboratory of Hydrology-Water Resources and Hydraulic Engineering, Hohai University, Nanjing 210098, China
[2] College of Agricultural Science and Engineering, Hohai University, Nanjing 210098, China
[3] Changjiang River Scientific Research Institute, Wuhan 430010, China
* Correspondence: xjz481@hhu.edu.cn

Abstract: The potential risk of flood or waterlogging in irrigation districts has increased due to global climate change and intensive human activities. This paper employed a waterlogging process simulation model for flat irrigation districts in the paddy fields to simulate floods under different scenarios. The scenarios of the rainfall conditions, initial storage depths, and work scales are designed, respectively. The risk of flood damage increases as rainfall increases, with a maximum increase of 62.8%, comparing the extreme scenario with the current scenario. A moderate rise in pumping station flow and using pre-rain drainage measures in the paddy fields can effectively reduce waterlogging loss. The total regional flood damage was reduced by up to 10.9%, 15.8%, and 35.9% when the pump station flow in the study area was increased by 10%, 20%, and 30%. The insights from this study of the possible future extreme flood events may help flood control planning.

Keywords: waterlogging; modeling; paddy field drainage; flood risk reduction

Citation: Liu, Z.; Xiong, Y.; Xu, J. Flood Simulation and Flood Risk Reduction Strategy in Irrigated Areas. *Water* **2023**, *15*, 192. https://doi.org/10.3390/w15010192

Academic Editor: Athanasios Loukas

Received: 26 November 2022
Revised: 22 December 2022
Accepted: 29 December 2022
Published: 2 January 2023

1. Introduction

Flood disaster commonly causes fatalities, socioeconomic damage, and damage to the natural environment [1–3]. The Sixth Assessment Report of the IPCC [4] points out that global climate change has significantly altered the global water cycle, increasing the frequency of extreme hydrological events such as heavy rainfall, flood, and drought, threatening social and economic development and ecosystem stability. Moreover, research indicates that the frequency and intensity of flooding are increasing [5–7]. The largest increases tend to occur in short-duration storms lasting less than a day, which could lead to an increase in the intensity and frequency of flash flooding [8,9]. Thus, the potential flood hazards and adverse impacts are larger. As reported in the literature, the size of extreme flood events increased by about 20%, and extreme flood event frequency increased by as high as 200%. As a result, flood risk increased by 30–127% [10]. Furthermore, flood risk and damage may increase with social development [11,12]; researchers have conducted a number of studies on flood risk assessment [13,14].

Agricultural systems are generally sensitive to flooding [15]. In agriculture-dominated countries, the extent of damage incurred on cropland by heavy and frequent floods is great. China has the world's largest population, and its arable land accounts for 7% of the world's arable land [16]. According to the Ministry of Water Resources of the People's Republic of China, the flooded area of crops reached 7190.0 thousand hectares, with a direct economic loss of 266.98 billion yuan, accounting for 0.26% of the GPD in 2020 [17]. Moreover, it can be confirmed that flood risk has increased in many places in China and is likely to grow further due to anthropogenic and climatic factors [18]. The number of extreme rains in the Yangtze River Basin's lower middle region is also increasing [19]. Given the importance of agriculture in the Chinese economy and its contribution to food production for a growing population, much more attention should be given to agricultural flood risk mitigation.

Other than extreme rainfall events, flood risk is also influenced by the landscape and anthropogenic activities. Accurate flood evolution simulation could provide scientific support for water security management in flat irrigation districts of plain river network regions [20,21]. It is a critical way to evaluate the flood risk and the performance of flood management practices. Several well-known hydrological models, such as the HEC-HMS/HEC-RAS model [22–24], the Xin'anjiang model [25], MIKE FLOOD [26], and the tank model [27,28], were used in flood simulation. Yet, these hydrological models generally worked well in natural watersheds [29] while less efficient in plain irrigation districts with artificial ditches and hydraulic structures. The calculation method of rainfall-runoff suitable for large-scale watersheds is not applicable in plain irrigation districts and needs to be improved. Researchers have tried this in many ways, Xiu and Wu [30] used MIKE II to develop a hydrodynamic model to analyze the hydrological conditions of the river courses in a plain river network system named the Ruiping water system. Liang [31] presented a whole basin hydrological system model for the Taihu lake drainage basin, which included five aspects: river and lake simulation, boundary condition simulation, rainfall and runoff simulation, engineering situation and control operation mode simulation, and water flow movement simulation in the main river network. Patel [32] assessed the flood and found inundation in low-lying areas of Surat city, Lower Tapi Basin, by using the HEC-RAS model and validated this for the year 2006. Chen [33] applied a distributed-framework basin modeling system (DFBMS) in the Taihu Basin. Hu [34] established a hydrologic and hydrodynamic processes model of the complex river network to simulate the rain-runoff processes of the rural and city regions in the Suzhou district, respectively. Nevertheless, plain irrigation districts have many variables with drainage works, complex river and lake networks, and frequent human interventions, making it difficult to simulate accurately. A hydrological model competent in simulating the flooding process with drainage works in the complex river network region is lacking. The tank model has been widely used in various terrain and climate conditions because of its simple principle and flexible structure. Studies have shown that the tank model can more accurately simulate the rainfall-runoff process in paddy fields and flat, low-lying agricultural areas [35,36]. Therefore, the tank model can be a useful tool for complex river network regions.

In the current research, with the Gaoyou irrigation District's flat and affluent river networks as a case, we conducted a scenario simulating analysis to investigate the flood risk under extreme rainfall. A Waterlogging Process Model for a flat irrigation district is applied to simulate the flooding process and flood loss for the flat irrigation district, and to schedule the optimal operation of drainage works under different simulation scenarios. An improved tank model and hydrodynamic model based on Saint-Venant equations are adopted in the runoff generation and confluence module, respectively. The waterlogging loss is calculated under inconstant inundated depth by linear interpolation. We simulated the flood risk response to rainfall with 10-year, 50-year, and 100-year return periods.

2. Study Areas

Gaoyou Irrigation District is a typical plain irrigation area of 650 km^2, located in Yangzhou, Jiangsu Province. The annual average rainfall is 1030 mm, and summer makes up about 50% of the yearly precipitation. We selected Longben Polder as one specific agricultural field of Gaoyou Irrigation District, of which the entire area is 26.6 km^2. It is high in the south and low in the west, and the flow direction is from south to north. The drainage system comprises the embankment, drainage ditch, barrier pond, river course, and gate station. The map of the study area and generalized drainage system is shown in Figure 1. The drainage system included seven pump stations with gates. The study area was divided into 23 field units with 32 nodes and 31 riverways (including hydraulic structures). The riverways connect by nodes. Each channel is divided into five equally spaced sections in the hydrodynamic calculation of the river network. All the pumping stations and culverts are generalized as river channels with a length of zero and numbered uniformly.

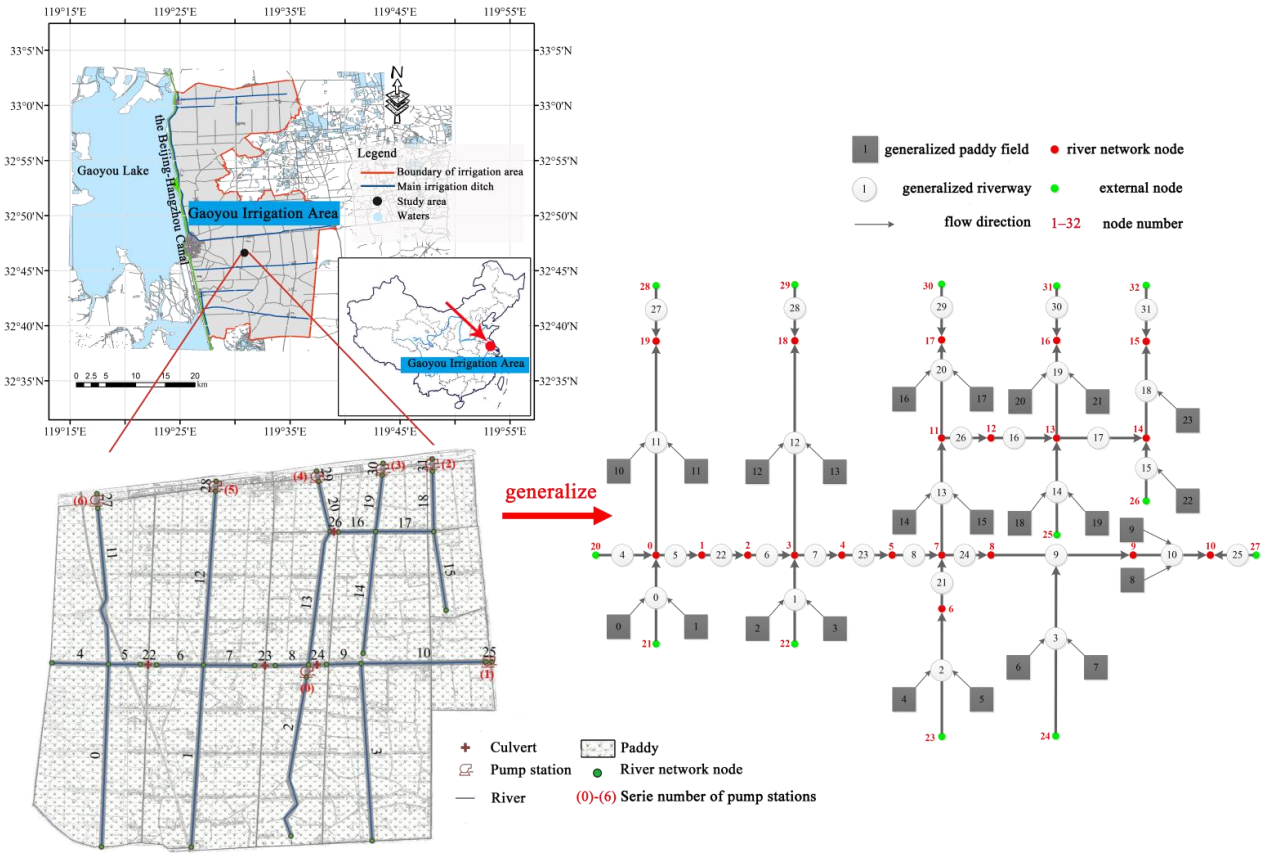

Figure 1. Study area map and drainage system generalization.

3. Methodology and Data

3.1. Waterlogging Process Model for the Paddy Fields

3.1.1. Framework and Assumptions of the Model

The Waterlogging Process Model was built [37] to simulate the flooding process and waterlogging loss for flat irrigation districts. This model was established by incorporating the hydrological model of the waterlogging process and the waterlogging loss estimation. The model of the waterlogging process was built based on a modified tank model and hydrodynamic model for the ditch-river system. The waterlogging loss is calculated under inconstant inundated depth by linear interpolation. Figure 2 shows the internal relationships between modules and their framework.

3.1.2. Waterlogging Process Simulation

The tank model simulated the rainfall-runoff process in the paddy fields. According to the hydrological and geological characteristics of the irrigated district, the rice field between two channels was regarded as a hydrological unit, and a two-layer tank model developed by Chen [36] was run on each unit. In the rainfall drainage process, the excess water from the paddy field was drained into the river channel through the outlet of the drainage ditch. Figure 3 shows the structure of the two-layer tank model.

In this model, the rice field drainage was uniformly drained into the canal or river along with the water flow and used as the side stream of the river channel. According to the study [28], the broad-crested weir overflow formula can be applied to calculate the paddy field discharge. Therefore, the submersed discharge formula and the free discharge formula of the broad-crested weir overflow formula were used to calculate the release from the side holes of the first layer of the tank model.

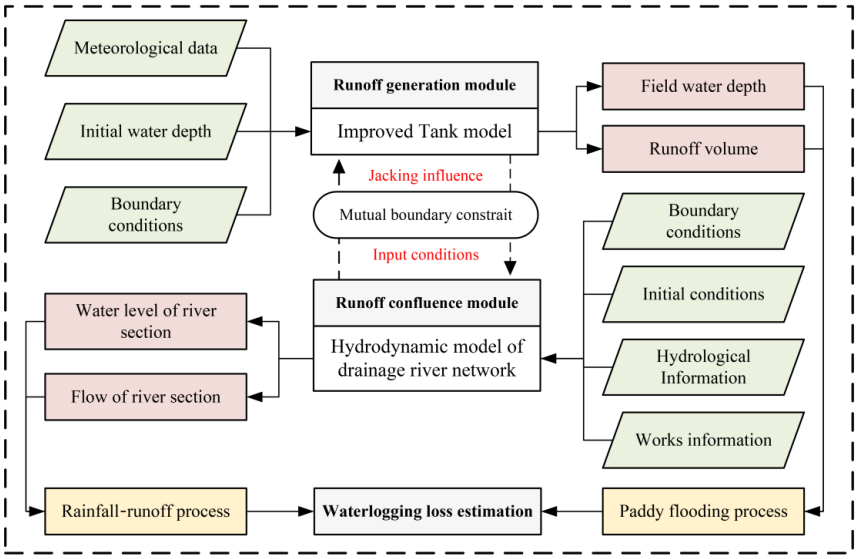

Figure 2. Framework and internal relationships between the modules of the Waterlogging Process Model.

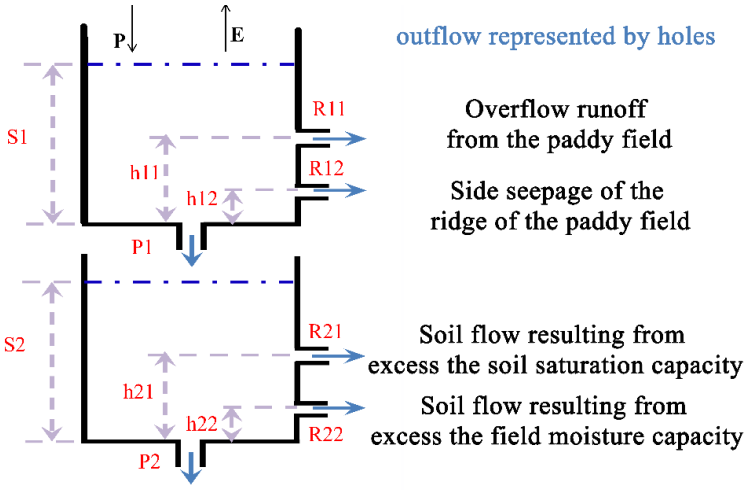

Figure 3. The structure and meaning of the two-layer tank model.

The 1D Saint-Venant equations [38] were used as the basic confluence equations of the plain river network. This paper uses Preissmann's implicit scheme to solve the Saint-Venant equations, including the dynamics and continuity equations.

This model was calibrated based on data collected, including the river water level, the paddy field runoff process, and the water storage depth in paddy fields. It confirms that the performance of the waterlogging process model is excellent. Detailed information for the model calibration can be found in an article by Xiong et al. 2021 [37].

3.1.3. Waterlogging Loss Estimation

The yield reduction rate in each unit was calculated as a function of the inundated water depth and the waterlogging process, according to the planting structure of crops in the study area. The total loss of waterlogging was calculated by multiplying the yield reduction rate with the local average yield and price. The mathematical expression of the waterlogging loss [39,40] in the stage of crop growth is as follows:

$$AD(i) = \sum_{k=1}^{n} [D_m(i,k) CRP_a(i,k) mn(k)] \quad (1)$$

$$D_m = CP_k F_k DC_k(i) \quad (2)$$

where AD is the total loss of farmland in the irrigated district, ten thousand Yuan; n is the number of crop species in the study area; D_m is economic losses of crop k per unit area in this flood, yuan/m^2; CRP_a—The planting area of crop k in cell i, hm^2; mn is the loss coefficient of crop k at different growth stages, mainly related to rice varieties; CP_k is the price of crop k, yuan/kg; F_k is the average yield of crop k, kg/m^2; DC_k is yield reduction rate of crop k per unit area (as a percentage of average annual yield), %, the detailed introduction and proof process can be found in an article by Liu [39,41].

3.1.4. Rules for Optimization of Drainage System Operation

Based on the Waterlogging Process Model, we developed a Model of Optimal Operation of Drainage Works (MOODW) to simulate and optimize the operation of drainage works. MOODW aims to minimize the sum of loss caused by waterlogging and energy cost of drainage works by scheduling the worktime of each pumping station and was solved by a genetic algorithm. It proved helpful in simulating the water flooding process and optimizing the drainage works operation. Hence, we applied this model in scenario simulation analysis to determine the optimal operation strategy before discussing the dynamics of flooding water and losses in the irrigation district's different scenarios. To match the actual operation practice, several rules for drainage works management were made as follows:

(1) Ignore the duration to open and close a specific drainage work; every drainage work is operated (open or close) once for one waterlogging event.

(2) All drainage works only have two states of fully opened and fully closed: the sluice is opened with an opening height above the water surface, or the pumping station is in operation at the rated flow. For the pump station with a gate, the pump is launched only when the gate is closed. A pump station with multiple pumps is considered one work.

(3) The flow rate and power consumption of a specific pump station are assumed to be constant and are calculated according to the rated value.

All the results for scenario simulation analysis, flooding water levels, and yield losses, illustrated in this article, are the data with the optimal operation strategy for multi-drainage works.

The Nash–Sutcliffe Efficiency Coefficient [42] was taken as an evaluation index of the hydrological models effectiveness, and an adaptive genetic algorithm was adapted for optimization [43]. Important parameters involved in the model, including calibrated parameters and fixed parameters, are shown in Table 1.

Table 1. Parameters in models.

Module	Parameters	Value	Source
Waterlogging process	h11, Height of upper hole in 1st layer	0.047 m	Calibration by measured rainfall data and water level data of the paddy field
	b1, b2, Weir width per unit area in 1st layer	b1:0.000014 m^{-1}; b2: 0.00076 m^{-1}	
	β1, Infiltration coefficient in1st layer	0.008	
	α21, α22, Outflow coefficient in 2nd layer	α21: 0.41 α22: 0.019	
	h21, h22, Height of upper hole in 2nd layer	h21: 0.50 m. h22: 0.40 m	
	β2, Infiltration coefficient in 2nd layer	0.032	
Waterlogging loss estimation	F_k	1.05 kg/m^2	Collected from Agricultural Bureau, Gaoyou, China
	CP_k	3 yuan/kg	
	$DC_{rice} = aH^bT^c$, H is the percentage of flooded water depth to plant height, %; T is flooded duration, day; a, b and c are parameters of the model.	a = 36.909, b = 2.084, c = 0.437	calibrated by data collected from Jiangsu Province, and the model was verified by Xiong [44]
Optimal operation	Generation Number	200	The parameter of the genetic algorithm refers to the research
	Individual Number	50	
	Chromosome Number	16	
	Mutation Rate	0.1	
	Crossover rate	0.6	

3.2. Scenario Setting

The Pearson-III curve was used to fit the extreme distribution of the maximum daily rainfall in Gaoyou [45,46], which was recommended by China's standard guidelines under the AM framework for a rainstorm and flood design [47]. In this paper, we collected the data from short-term rainstorms from 1971 to 2012 in the Gaoyou Irrigation District from the National Meteorological Information Center (https://data.cma.cn/, accessed on 13 January 2019.) of the China Meteorological Administration and applied it for statistical analysis. According to the standard for flood control in the agricultural polder area of Gaoyou, three levels of extreme rainfall were selected: 100-year return periods (1% frequency), 50-year return periods (2% frequency), and 20-year return periods (5% frequency).

Thus, the Gaoyou irrigation district had high and concentrated rainfall characteristics. Calculation results according to the Pearson-III curve were presented as contour maps to describe the daily rainfall characteristics in 20, 50, and 100-year return periods, with maximum daily rainfall of 196.1, 228.41, and 250.46 mm. The maximum 1, 3, 6, and 24-h rainfall in 1976 occurred simultaneously from 5:00 on June 29 to 5:00 on 30 June 1976. Therefore, this hour-by-hour rainfall process was selected as a typical rainstorm process. The calculation results and typical rainfall process distribution map are shown in Figure 4.

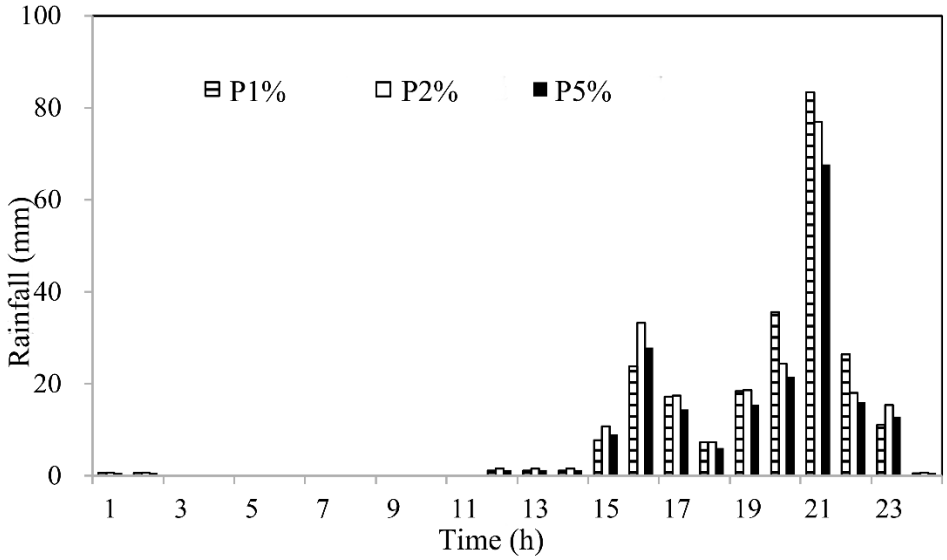

Figure 4. Time distribution diagram of a typical rainfall process.

Studies have shown that the 24-h extreme rainfall in China will increase by 10% to 20% every 10 years [48,49]. Therefore, we set a scenario of extreme rainfall that increased by 15% on top of the current precipitation. The maximum extreme 24-h rainfall of 20, 50, and 100-year return periods in the Gaoyou irrigation area is 225.52 mm, 262.67 mm, and 288.03 mm, respectively.

The moisture condition before rainfall affects the water storage capacity of the paddy fields, which involves confluence and waterlogging in the irrigation districts [50]. In this paper, we considered two paddy field moisture states: the state of no water layer before irrigation and the state of water layer after irrigation. Therefore, we set scenarios of initial paddy water storage depths at 0 cm and 3 cm, respectively. Based on the current scale of drainage works, we designed three ampliative pump station flow rates, which are 110%, 120%, and 130%, respectively. Rice is sensitive to waterlogging at the jointing and booting stages [51,52], so the loss evaluation in all scenarios is carried out at the jointing and booting stage. The initial water level of the outer river was assumed to be 1.5 m (the average water level of the local outer river).

4. Results and Discussion

4.1. Paddy Loss under Current and Extreme Rainfall

In the jointing and booting stage of rice, waterlogging losses were simulated under different rainfall frequencies at an initial filed water layer of 3 cm. The drainage works in the study area meet the standard of a 20-year return period.

When rainfall occurs in a 20-year return period, the irrigation district can avoid waterlogging loss by proper scheduling (Figure 5a). In this case, the flooded depth of paddy fields did not reach the critical depth of flood disaster at the jointing and booting stage. However, as seen in Figure 5, the flooded depth increased rapidly with rainfall. The maximum flooded water depth under the 100-year return period increased by 2 cm and 7 cm, respectively, compared with that of 50-year and 20-year return periods.

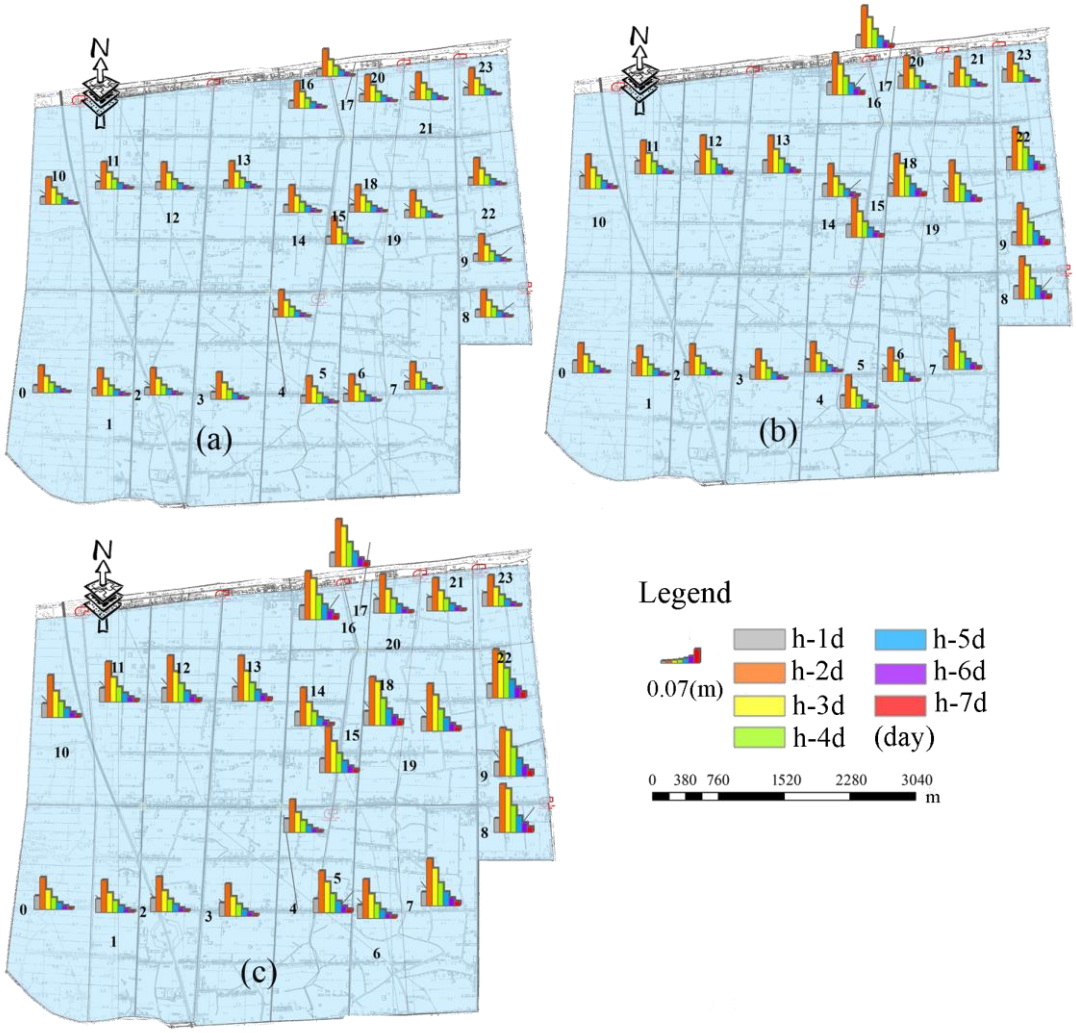

Figure 5. Variation and distribution of submerged depth under different rainfall return periods of the current scenario ((**a**). P5% (**b**). P2% (**c**). P1%, unit: m).

The waterlogging loss of paddy fields increased by about 20% in the case of the 100-year return period compared to the 50-year return period. Figure 6 analyzed the yield loss of paddy fields under different rainfall conditions. The 20-year return period rainfall did no damage, while the waterlogging loss under the 50-year return period and the 100-year return period were 49.2–141.8 $\times$ 10^3 yuan/km^2 and 52.2–197.0 $\times$ 10^3 yuan/km^2, respectively.

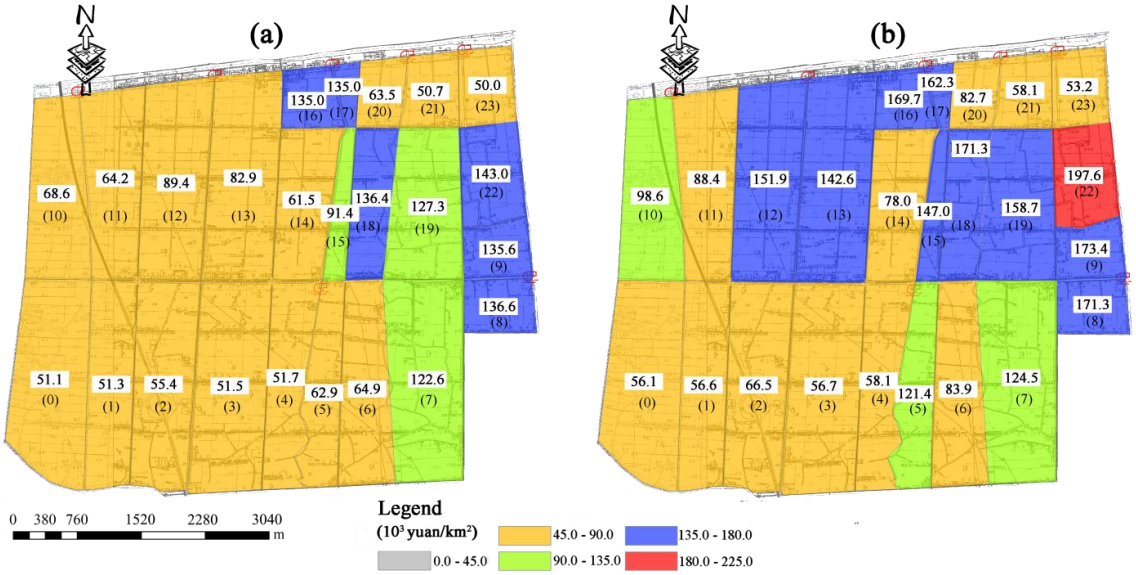

Figure 6. Waterlogging loss under different rainfall return periods of the current scenario ((**a**). P2% (**b**). P1%).

Figure 7 shows that as rainfall increased, the area of the paddy fields suffered waterlogging loss. Comparing Figures 6 and 7, the waterlogging losses on paddy fields due to different rainfall frequencies in the extreme climate were more severe. When the rainfall return period is 20 years, there is no loss in the current rainfall scenario, and in the extreme scenario, it is 49.3–123.9 $\times$ 10^3 yuan/km^2. However, Waterlogging loss increased from 50.7–143.3 $\times$ 10^3 yuan/km^2 in the present scenario to 58.2–204.5 $\times$ 10^3 yuan/km^2 in the extreme scenario when 50-year rainfall occurred. While with the 100-year rainfall, the waterlogging loss increased to 68.7–331.3 $\times$ 10^3 yuan/km^2 in the extreme scenario, with a maximum increase of 62.8%. Table 1 analyzes the difference between farmland flood losses under extreme and current conditions.

With 20-year, 50-year, and 100-year return periods of extreme rainfall, the summed waterlogging loss in the study area was 1.95 million, 3.13 million, and 4.82 million yuan, respectively (Table 2). When rainfall increases by 15%, the loss of waterlogging caused by 20-year rainfall is almost equivalent to that caused by 50-year rainfall in the current. In contrast, the loss caused by 50-year rainfall is virtually comparable to that caused by 100-year rainfall in the current.

For drainage works, in the same scenario, the total operating hours increased significantly as the return period increased. For example, when the return period changed to 100-year from 20-year, the entire pump operating hours increased by 49.6% in the extreme scenario, compared to 44.5% in the current scenario (Figure 8). Therefore, with future climate change, the risk of flood damage increases as extreme rainfall increases. Assuming the drainage works remain the same, the extremes in rainfall lead to lower flood mitigation standards. In other words, the drainage pressure of the existing drainage works is growing.

4.2. Effects of Initial Storage Depths on Flood Removal

To understand the mechanism of the influence of initial storage depth on field storage depth and yield reduction, four typical fields in different directions of the study area were selected. Figure 9 analyzed the variation patterns of the waterlogging depth and the yield reduction rate of paddy fields with different initial water storage when encountering a current 50-year rainfall. From the figure, the four typical fields showed a consistent pattern, while the effect of the water storage depth on paddy fields 9 and 22 was more evident that the inundation loss of paddy fields is doubled when there is a water layer compared with no water layer. The inundation depth experienced a rapid increase to a gradual decrease, while the inundation depth of paddy fields with aquifers was always higher than that of

paddy fields without aquifers. The cumulative yield reduction rate increased with the inundation depth and remained constant after reaching the peak. Therefore, the initial water layer increased the submerged depth and prolonged the submerged time of the paddy field.

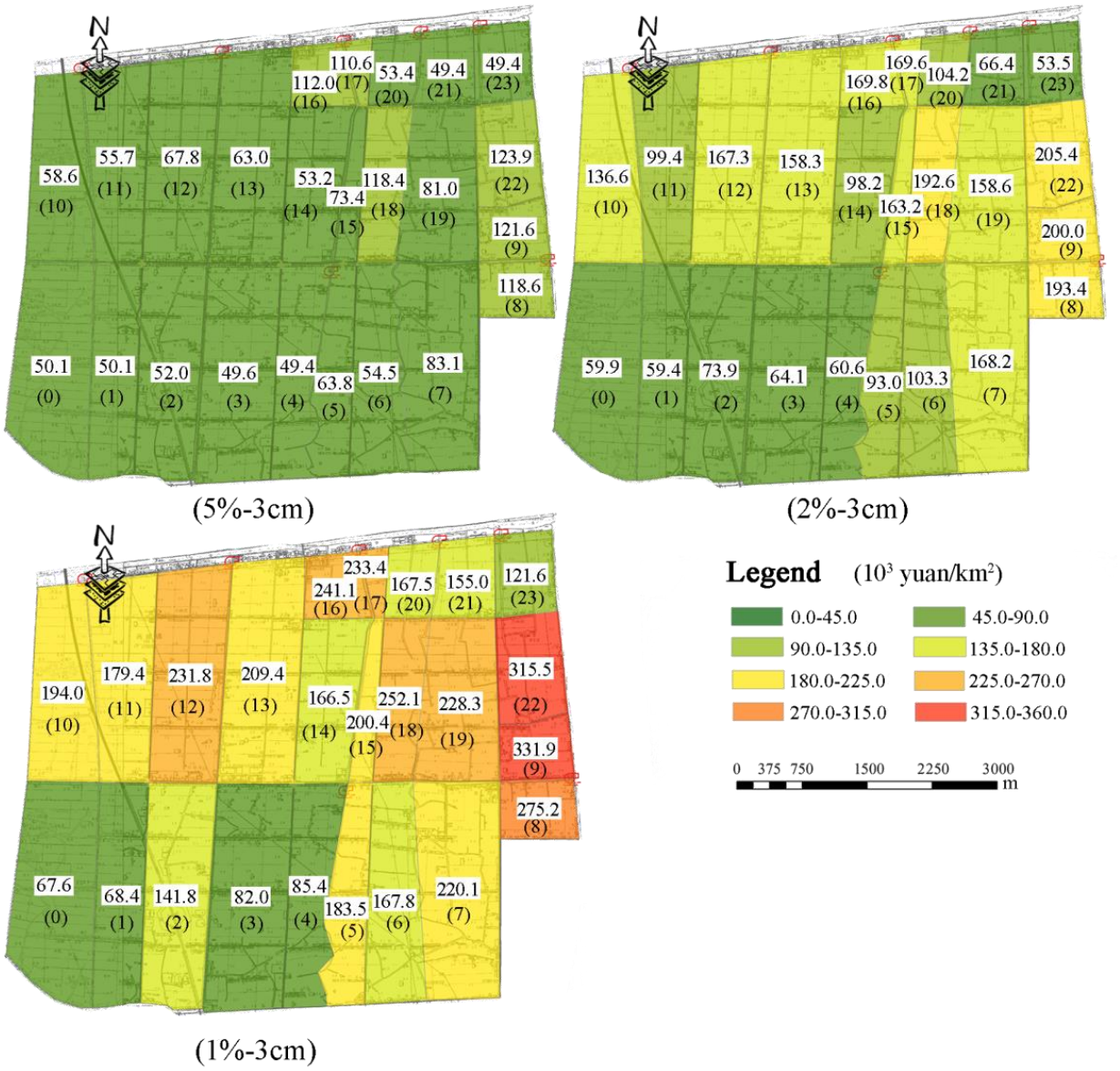

Figure 7. Distribution of waterlogging loss under different rainfall return periods of extreme scenario.

Table 2. Waterlogging loss under extreme and current rainfall conditions (unit: 10^3 yuan).

Scenario	Frequency	Crop Loss	Pump Fee	Total Loss
Extreme	5%	1881.2	69.6	1950.8
	2%	3039.3	97.7	3137
	1%	4709.2	109.0	4818.2
Current	5%	0	56.5	56.5
	2%	2261.7	69.2	2330.9
	1%	2772.7	88.2	2860.9

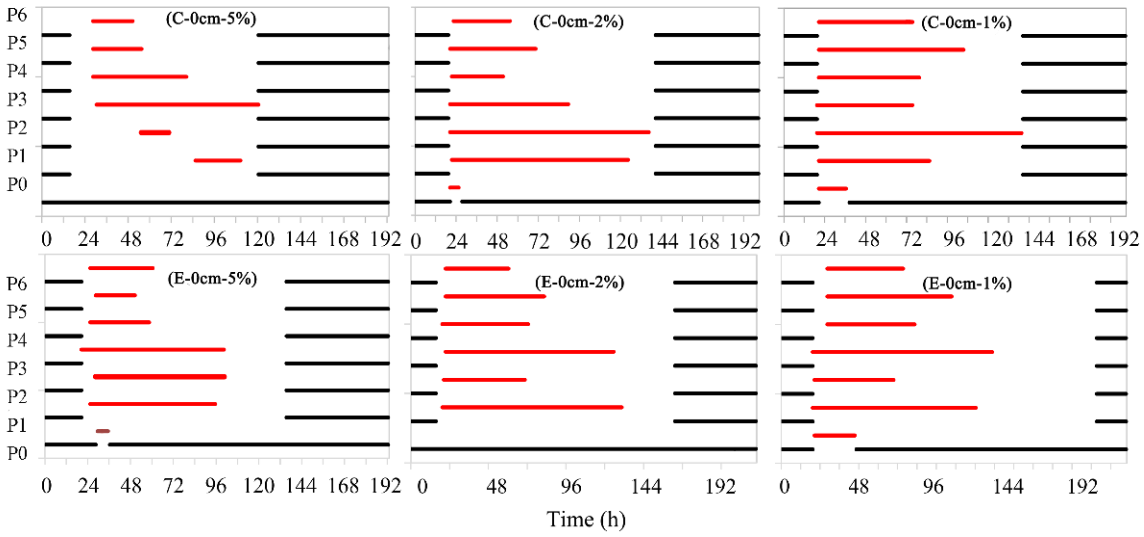

Figure 8. Scheduling schemes under different frequency rainfall conditions in the current and extreme climate scenario. Black represents the gate and red represents the pump. Serial number of pump Station: P0: Heping, P1: Zhongxinhe, P2: Nijia, P3: Hongqi, P4: Jiangmahe, P5: Zhongshihe, P6: Lvyanghe. C: current scenario, E: extreme scenario.

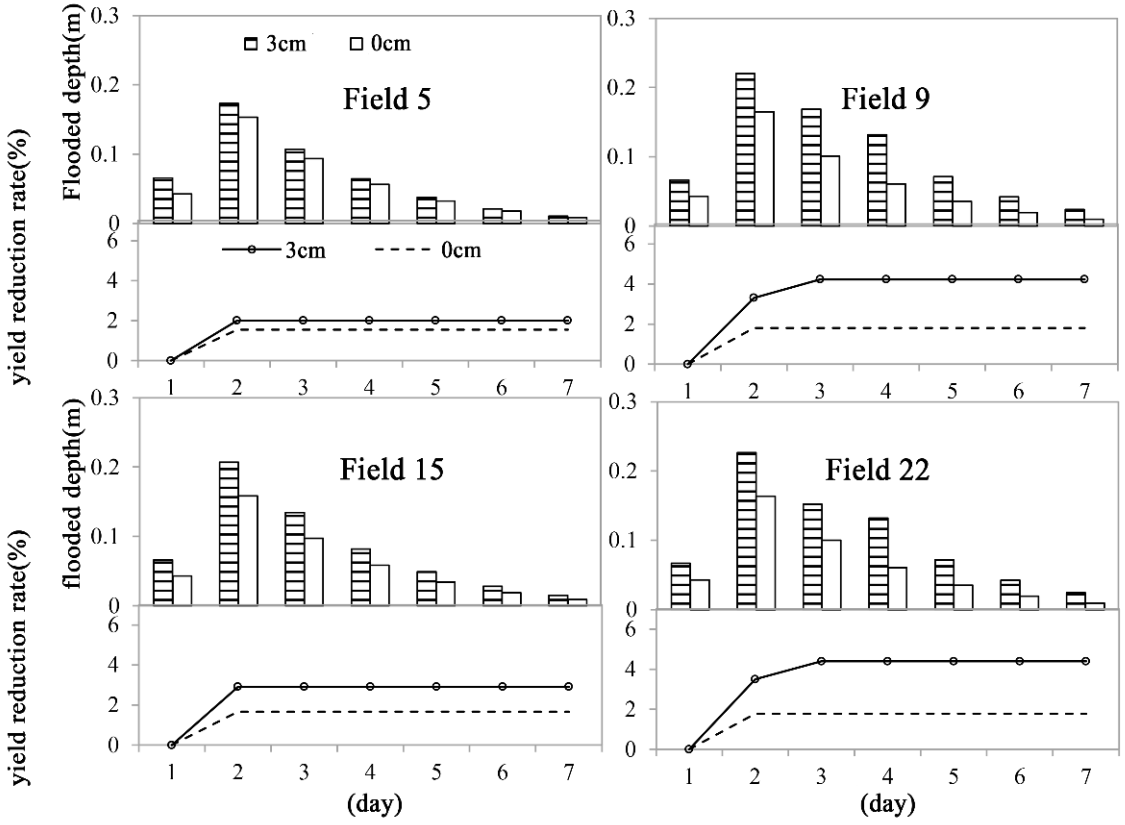

Figure 9. Variation of waterlogging depth and yield reduction rate of paddy fields with different initial storage depths under a 50-year rainfall of the current scenario.

Table 3 compares the waterlogging losses between paddy fields with and without water storage in the status quo scenario. It can be concluded that keeping paddy fields free of water before rainfall reduces the likelihood and severity of flooding and the pump fee decreases.

Table 3. Waterlogging loss of study area under different initial storage depths in the current condition (unit: 10^3 yuan).

Scenario (a-b [1])	Crop Loss	Pump Fee	Total Loss
5%-0	0.0	43.3	43.3
5%-3	0.0	56.5	56.5
2%-0	1447.2	67.0	1514.1
2%-3	2261.7	69.2	2330.9
1%-0	1801.8	86.6	1888.4
1%-3	2772.7	88.2	2860.9

Note: a: rainfall frequency; b: initial storage depth.

In the event of 50-year and 100-year rainfall, the waterlogging loss of paddy fields without water storage was reduced by 35% and 34%, respectively, compared with the 3 cm initial water level. Paddy fields are similar to reservoirs when it rains; the rainfall is first stored in the paddy field, and only when a certain amount of water is stored it produces flow. Keeping the paddy field free of water before rainfall increases the space for storing water in the paddy field and helps relieve the pressure of flooding. Therefore, pre-draining before rain or reducing the time of paddy water accumulation can effectively reduce the risk of waterlogging loss.

As the rainfall increases by 15%, the distribution of flood damage in paddy fields without the initial water layer under extreme rainfall conditions is shown in Figure 10. In the case of no water layer, the waterlogging loss was 48.9 yuan/km^2 for a 20-year rainfall, 50.7 to 152.5 yuan/km^2 for a 50-year rainfall, and 61.0 to 225.6 yuan/km^2 for a 100-year rainfall, respectively. Comparing Figures 7 and 10, the waterlogging losses of paddy fields without a water layer were significantly less than those of paddy fields with an initial water layer of 3 cm under the same rainfall conditions. Keeping the waterless layer before rain can reduce 26.7% of flood damage compared with a 3 cm water layer as the frequency of rainfall is 5%; for 2% and 1% frequency rainfall, it decreased by 32.7% and 23.2%, respectively.

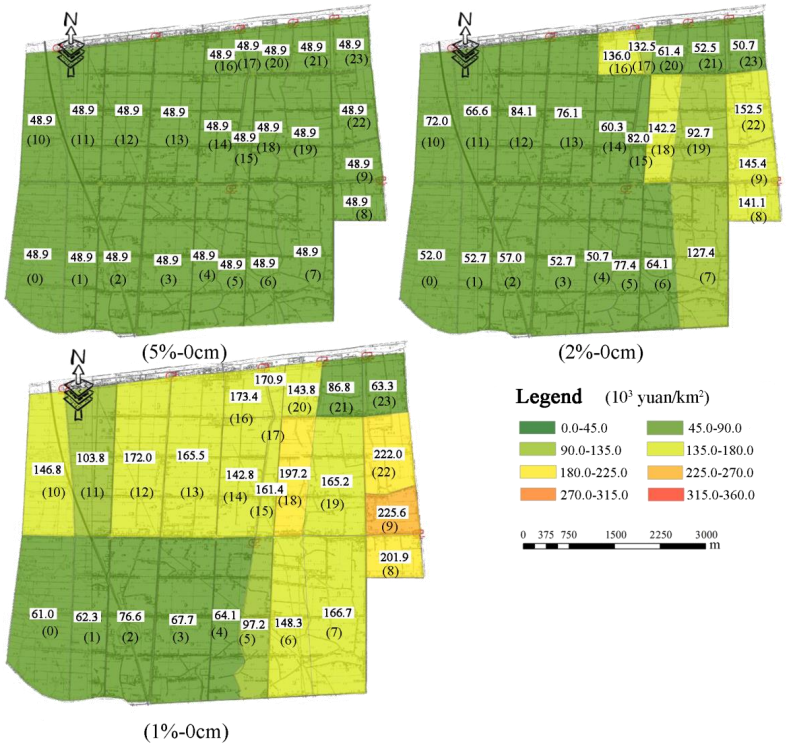

Figure 10. Waterlogging loss of paddy fields with an initial storage depth of 0 cm under different rainfall frequencies.

Meanwhile, comparing Figures 8 and 11 showed that the operating time of the pump stations and gates of 0 cm initial depth was significantly shorter than that of 3 cm initial depth. Therefore, proper pre-rainfall paddy-water layer management can reduce regional waterlogging losses. Pre-drainage before rain increases the rainfall storage capacity of paddy fields, thus effectively intercepting rainfall and reducing the drainage of paddy fields.

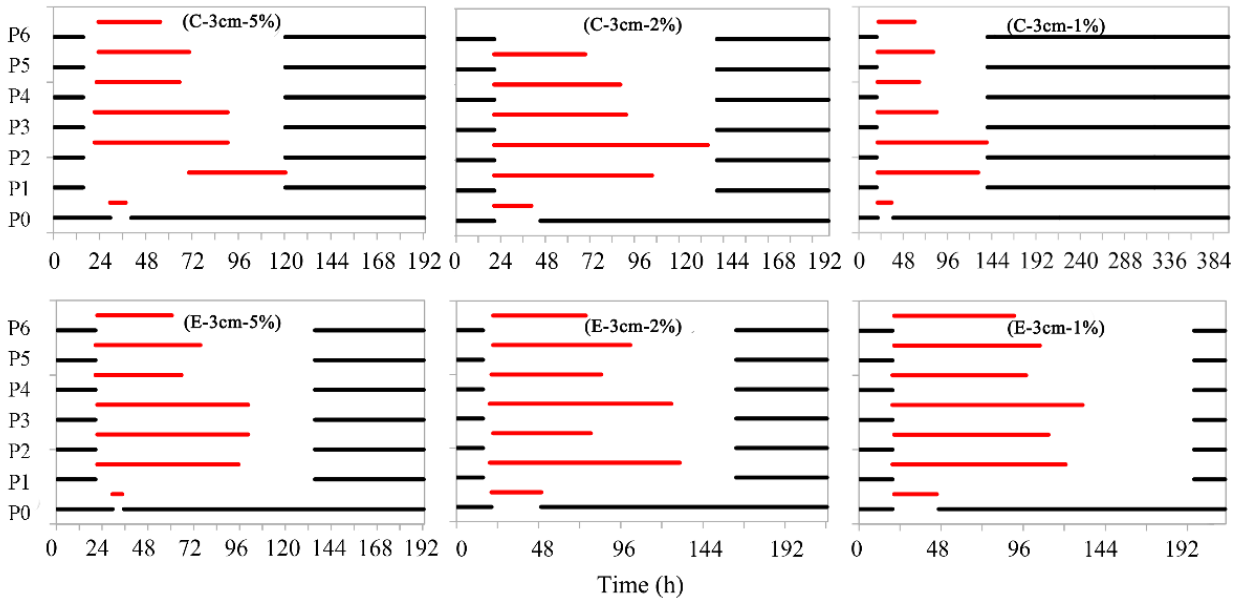

Figure 11. Scheduling schemes under different frequency rainfall conditions in the current and extreme climate scenario (initial storage depth of 0 cm).

4.3. Effects of Drainage Capacity on Flood Removal

Figure 12 shows the scheduling schemes of different work scales and initial water storage depths under 20-year, 50-year, and 100-year rainfall events. With the same initial water depth and rainfall frequency, the more the work scale is increased, the shorter the time required to operate the pump station. Still, the pump fee is likely more expensive because the bigger work scale requires a higher hourly operating cost. Therefore, scaling up the project requires a comprehensive estimation of efficiency and overall cost.

Based on 50-year and 100-year rainfall events under extreme rainfall scenarios, Figures 13 and 14 showed the effect of work scale and the depth of the initial water layer on waterlogging loss. The average waterlogging loss per km^2 tended to decrease with the increase in the scale of flood drainage works. For example, when paddy fields with an initial water layer of 0 cm were subjected to a 50-year rainfall event, the average losses per km^2 were reduced by 6.9%, 11.9%, and 17.7% when the drainage flow of pump stations was increased by 10%, 20% and 30%, respectively, compared with the waterlogging loss of the current work scale. Furthermore, the average losses per km^2 with an initial water layer of 3 cm were 5.1%, 9.9%, and 15.8% lower than the status quo scale, respectively.

In the event of 100-year rainfall, the effects of the scale of the works on waterlogging loss mitigation were more prominent. For example, for Paddy field 22, with an initial water layer of 3 cm, which was most severely affected, the average losses per km^2 were reduced by 11.2%, 16.1%, and 40.9% when the work scale was increased by 10%, 20% and 30%, respectively, compared with that of the current work scale. From Table 4, overall, the total loss for a 1% frequency of extreme rainfall at an initial water layer of 3 cm and a 10%, 20%, and 30% increase in pump station flow in the study area was 4.373 million, 4.241 million and 3.144 million yuan, which were 10.6%, 13.2% and 35.0% less than the total loss of 4.999 million yuan at the status quo scale, respectively.

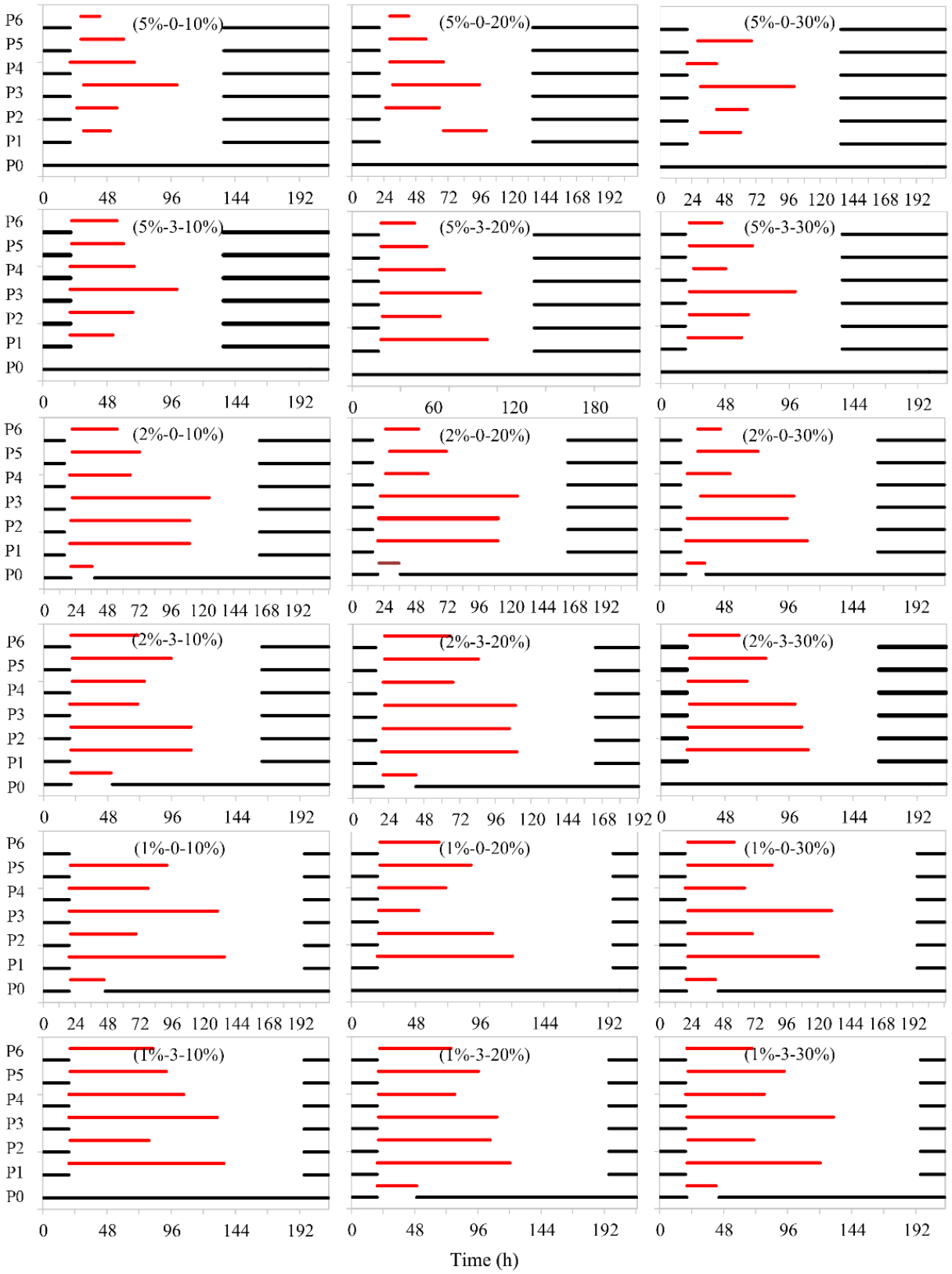

Figure 12. Scheduling schemes under different frequency rainfall conditions and work scale in the extreme climate scenario. (a–c, a: rainfall frequency, b: initial water level, c-work scale increased).

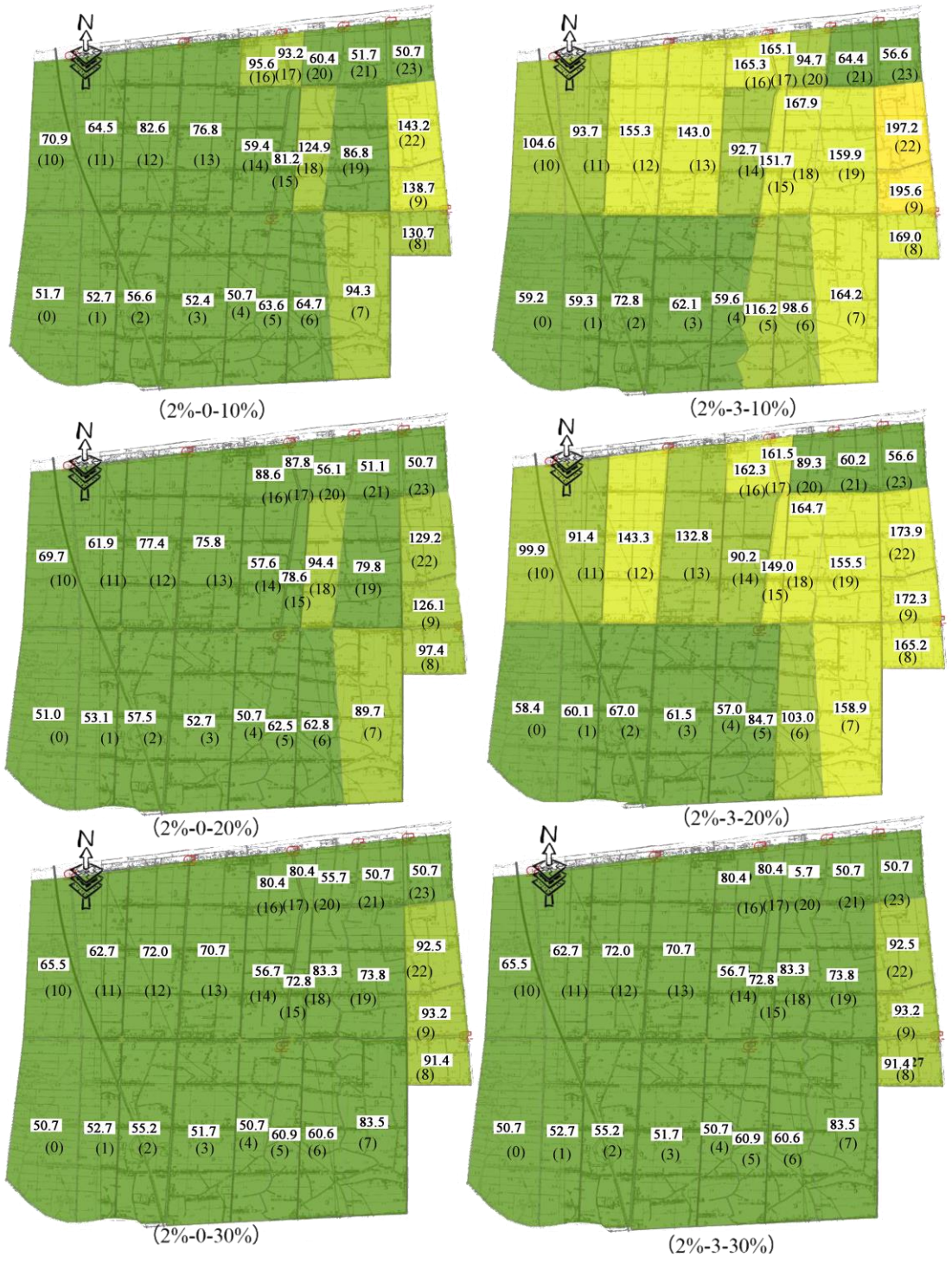

Figure 13. Distribution of averaged waterlogging loss with different initial storage depths and work scales under 2% frequency.

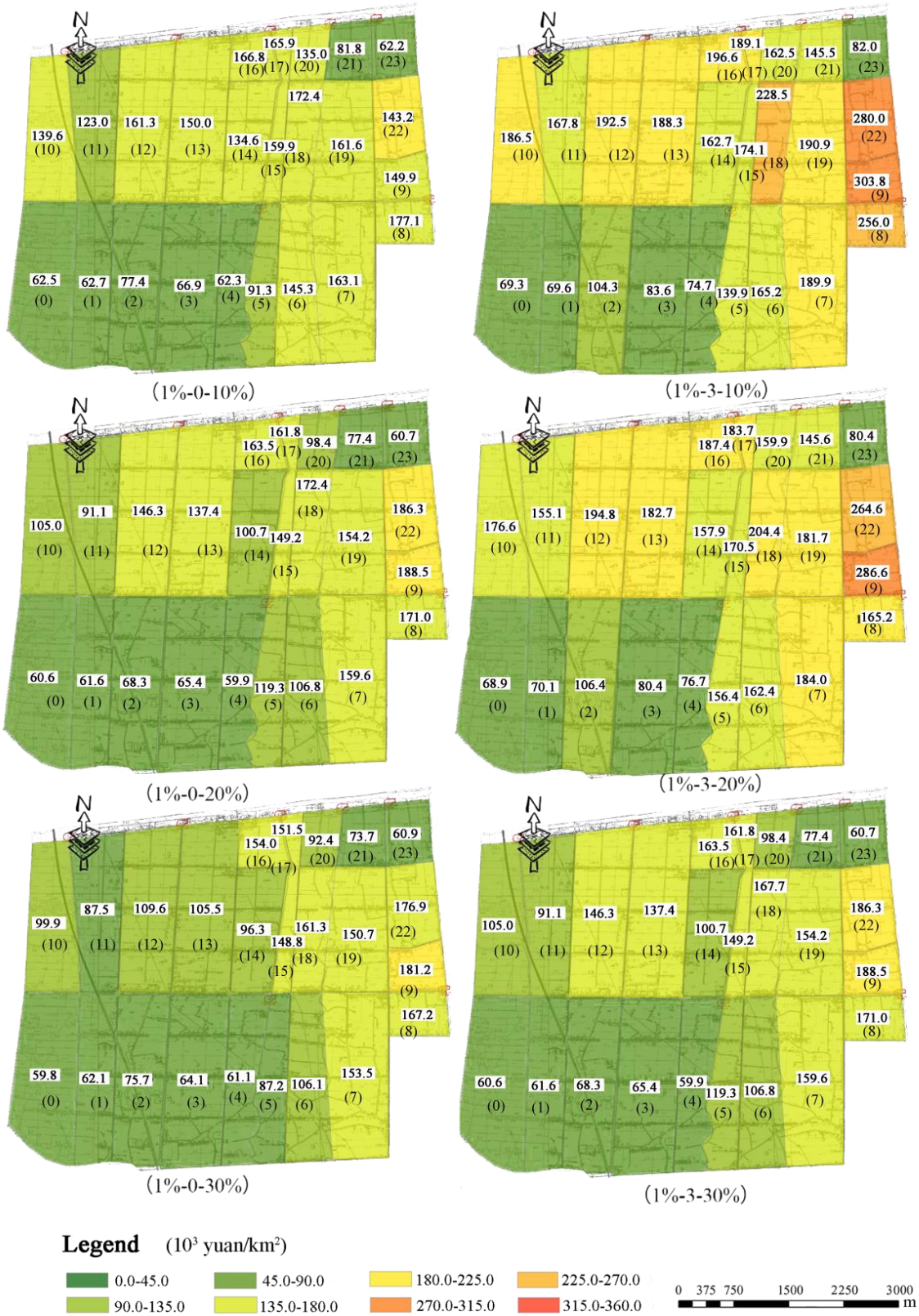

Figure 14. Distribution of averaged waterlogging loss with different initial storage depths and work scales under 1% frequency.

Table 4. Waterlogging loss under different conditions.

Scenario			Waterlogging Loss (10^3 Yuan)		
Work Scale	**Initial Storage Depth**	**Rainfall Frequency**	**Pump Fee**	**Crop Loss**	**Total Loss**
current	3 cm	5%	69.6	1881.2	1950.8
		2%	97.7	3339.3	3437.0
		1%	109.0	4909.2	5018.2
	0 cm	5%	52.4	1377.5	1429.8
		2%	77.4	2234.4	2311.8
		1%	90.6	3610.5	3701.1
Increased by 10%	3 cm	5%	59.3	1837.8	1897.1
		2%	95.5	3168.1	3263.6
		1%	108.4	4373.1	4481.5
	0 cm	5%	45.9	1307.5	1353.4
		2%	82.2	2081.2	2163.4
		1%	100.9	3451.2	3552.1
Increased by 20%	3 cm	5%	65.6	1748.9	1814.5
		2%	97.4	3007.9	3105.3
		1%	113.3	4241.4	4354.7
	0 cm	5%	47.8	1271.5	1319.2
		2%	79.6	1968.1	2047.6
		1%	90.1	3144.4	3234.5
Increased by 30%	3 cm	5%	62.7	1628.1	1690.8
		2%	92.5	2810.2	2902.7
		1%	115.6	3144.4	3260.0
	0 cm	5%	48.4	1209.6	1257.9
		2%	77.6	1837.8	1915.4
		1%	101.8	2920.3	3022.1

Thus, combining water layer control and pumping station capacity improvement can effectively relieve flood damage.

5. Conclusions

The present study modeled the hydrologic and hydrodynamic processes of the complex river network in the Gaoyou district. Based on the observed data and existing research, the current flood control planning scenarios and the extreme condition are designed, respectively. It can be concluded that the combined application of flood process simulation, flood loss estimation, and operation optimization scheduling, can simulate and optimize the scheduling of multi-drainage projects and achieve disaster reduction.

In general, climate change increases the frequency uncertainty of heavy rainfall and increases the potential risk of flood in irrigated districts. For example, when rainfall increases by 15%, the growth of waterlogging loss is up to 62.8% compared to the current. Therefore, we simulated the effects of two mitigation strategies. The result indicated that a moderate increase in the flow of pumping stations for flood removal in irrigation districts and using pre-rain drainage measures in rice fields could effectively reduce waterlogging losses. In addition, the combination of the two strategies can achieve better results.

Thus, strengthening the capacity of drainage works and taking appropriate field water management measures help to reduce the impact of future extreme floods. The results can provide a reference for the drainage works construction planning. The modeling approach and the evaluation parameters are practical for the flood severity estimation of the catchment, similar to the Gaoyou District. Future studies should focus more on the difference in runoff characteristics of different land use forms, or the combined impact of other flood mitigation measures.

Author Contributions: Conceptualization, Z.L. and Y.X.; methodology, Z.L.; software, Z.L.; validation, Z.L., Y.X. and J.X.; formal analysis, Z.L.; investigation, Z.L.; resources, Z.L.; data curation,

Y.X.; writing—original draft preparation, Z.L.; writing—review and editing, J.X.; visualization, Z.L.; supervision, Z.L.; project administration, J.X.; funding acquisition, Y.X. and J.X. All authors have read and agreed to the published version of the manuscript.

Funding: This work was supported by the National Natural Science Foundation of China (U2040213), the Fundamental Research Funds for the Central Universities (B210205014), the National Key Research and Development Program of China (2018YFC1508303), the Science Foundation of Jiangxi Provincial Water Conservancy Department in China (202022ZDKT07, 202124ZDKT09).

Institutional Review Board Statement: Not applicable.

Informed Consent Statement: Not applicable.

Data Availability Statement: The data that support the findings of this study are available on request from the corresponding author.

Acknowledgments: The authors wish to extend profound gratitude to research Group on Efficient Water Saving, Hohai University.

Conflicts of Interest: The authors declare no conflict of interest.

References

1. Wijayanti, P.; Zhu, X.Q.; Hellegers, P.; Budiyono, Y.; van Ierland, E.C. Estimation of river flood damages in Jakarta, Indonesia. *Nat. Hazards* **2017**, *86*, 1059–1079. [CrossRef]
2. Dellapenna, T.M.; Hoelscher, C.; Hill, L.; Critides, L.; Salgado, V.; Bell, M.; Al Mukaimi, M.E.; Du, J.B.; Park, K.; Knap, A.H. Hurricane Harvey Delivered a Massive Load of Mercury-Rich Sediment to Galveston Bay, TX, USA. *Estuaries Coasts* **2022**, *45*, 428–444. [CrossRef]
3. Siegel, H.; Gerth, M. Satellite-based studies of the 1997 Oder flood event in the southern Baltic Sea. *Remote Sens. Environ.* **2000**, *73*, 207–217. [CrossRef]
4. IPCC. *2021: Climate Change 2021: The Physical Science Basis. Contribution of Working Group I to the Sixth Assessment Report of the Intergovernmental Panel on Climate Change*; Masson-Delmotte, V., Zhai, P., Pirani, A., Connors, S., Péan, C., Berger, S., Caud, N., Chen, Y., Goldfarb, L., Gomis, M., et al., Eds.; Cambridge University Press: Cambridge, UK; New York, NY, USA; 2391p. [CrossRef]
5. Risser, M.D.; Wehner, M.F. Attributable Human-Induced Changes in the Likelihood and Magnitude of the Observed Extreme Precipitation during Hurricane Harvey. *Geophys. Res. Lett.* **2017**, *44*, 12457–12464. [CrossRef]
6. Kong, F.; Shi, P.; Fang, J.; Lu, L.; Fang, J.; Guo, J. Advances and Prospects of Spatiotemporal Pattern Variation of Extreme Precipitation and its Affecting Factors under the Background of Global Climate Change. *J. Catastrophology* **2017**, *32*, 165–174.
7. Prein, A.F.; Rasmussen, R.M.; Ikeda, K.; Liu, C.H.; Clark, M.P.; Holland, G.J. The future intensification of hourly precipitation extremes. *Nat. Clim. Change* **2017**, *7*, 48–52. [CrossRef]
8. Westra, S.; Fowler, H.J.; Evans, J.P.; Alexander, L.V.; Berg, P.; Johnson, F.; Kendon, E.J.; Lenderink, G.; Roberts, N.M. Future changes to the intensity and frequency of short-duration extreme rainfall. *Rev. Geophys.* **2014**, *52*, 522–555. [CrossRef]
9. Moustakis, Y.; Papalexiou, S.M.; Onof, C.J.; Paschalis, A. Seasonality, Intensity, and Duration of Rainfall Extremes Change in a Warmer Climate. *Earth Future* **2021**, *9*, 15. [CrossRef]
10. Swain, D.L.; Wing, O.E.J.; Bates, P.D.; Done, J.M.; Johnson, K.A.; Cameron, D.R. Increased Flood Exposure Due to Climate Change and Population Growth in the United States. *Earth Future* **2020**, *8*, 17. [CrossRef]
11. Reynard, N.S.; Kay, A.L.; Anderson, M.; Donovan, B.; Duckworth, C. The evolution of climate change guidance for fluvial flood risk management in England. *Prog. Phys. Geogr.* **2017**, *41*, 222–237. [CrossRef]
12. Chen, L.-n.; Zhao, Z.-l.; Guo, G.-m.; Li, J.; Wu, W.-b.; Zhang, F.-x.; Zhang, X. Effects of muddy water irrigation with different sediment gradations on nitrogen transformation in agricultural soil of Yellow River Basin. *Water Sci. Eng.* **2022**, *15*, 228–236. [CrossRef]
13. Stefanidis, S.; Alexandridis, V.; Theodoridou, T. Flood Exposure of Residential Areas and Infrastructure in Greece. *Hydrology* **2022**, *9*, 145. [CrossRef]
14. Qiang, Y. Flood exposure of critical infrastructures in the United States. *Int. J. Disaster Risk Reduct.* **2019**, *39*, 101240. [CrossRef]
15. Shrestha, B.B.; Okazumi, T.; Miyamoto, M.; Sawano, H. Flood damage assessment in the Pampanga river basin of the Philippines. *J. Flood Risk Manag.* **2016**, *9*, 355–369. [CrossRef]
16. Piao, S.L.; Ciais, P.; Huang, Y.; Shen, Z.H.; Peng, S.S.; Li, J.S.; Zhou, L.P.; Liu, H.Y.; Ma, Y.C.; Ding, Y.H.; et al. The impacts of climate change on water resources and agriculture in China. *Nature* **2010**, *467*, 43–51. [CrossRef]
17. Ministry of Water Resources of the People's Republic of China. *2020 Bulletin on Flood and Drought Disaster Prevention in China*; 27 September 2021; Ministry of Water Resources of the People's Republic of China: Beijing, China, 2021.
18. Kundzewicz, Z.W.; Su, B.D.; Wang, Y.J.; Xia, J.; Huang, J.L.; Jiang, T. Flood risk and its reduction in China. *Adv. Water Resour.* **2019**, *130*, 37–45. [CrossRef]

19. Han, L.F.; Xu, Y.P.; Pan, G.B.; Deng, X.J.; Hu, C.S.; Xu, H.L.; Shi, H.Y. Changing properties of precipitation extremes in the urban areas, Yangtze River Delta, China, during 1957-2013. *Nat. Hazards* **2015**, *79*, 437–454. [CrossRef]
20. Samantaray, D.; Chatterjee, C.; Singh, R.; Gupta, P.K.; Panigrahy, S. Flood risk modeling for optimal rice planning for delta region of Mahanadi river basin in India. *Nat. Hazards* **2015**, *76*, 347–372. [CrossRef]
21. Li, W.J.; Xu, B.; Wen, J.H. Scenario-based community flood risk assessment: A case study of Taining county town, Fujian province, China. *Nat. Hazards* **2016**, *82*, 193–208. [CrossRef]
22. Knebl, M.R.; Yang, Z.L.; Hutchison, K.; Maidment, D.R. Regional scale flood modeling using NEXRAD rainfall, GIS, and HEC-HMS/RAS: A case study for the San Antonio River Basin Summer 2002 storm event. *J. Environ. Manag.* **2005**, *75*, 325–336. [CrossRef]
23. Farooq, M.; Shafique, M.; Khattak, M.S. Flood hazard assessment and mapping of River Swat using HEC-RAS 2D model and high-resolution 12-m TanDEM-X DEM (WorldDEM). *Nat. Hazards* **2019**, *97*, 477–492. [CrossRef]
24. Horritt, M.S.; Bates, P.D. Evaluation of 1D and 2D numerical models for predicting river flood inundation. *J. Hydrol.* **2002**, *268*, 87–99. [CrossRef]
25. Hu, C.H.; Guo, S.L.; Xiong, L.H.; Peng, D.Z. A modified Xinanjiang model and its application in northern China. *Nord. Hydrol.* **2005**, *36*, 175–192. [CrossRef]
26. Patro, S.; Chatterjee, C.; Mohanty, S.; Singh, R.; Raghuwanshi, N.S. Flood Inundation Modeling using MIKE FLOOD and Remote Sensing Data. *J. Indian Soc. Remote Sens.* **2009**, *37*, 107–118. [CrossRef]
27. Hashino, M.; Yao, H.; Yoshida, H. Studies and evaluations on interception processes during rainfall based on a tank model. *J. Hydrol.* **2002**, *255*, 1–11. [CrossRef]
28. Chen, R.S.; Pi, L.C.; Huang, Y.H. Analysis of rainfall-runoff relation in paddy fields by diffusive tank model. *Hydrol. Process.* **2003**, *17*, 2541–2553. [CrossRef]
29. Uniyal, B.; Dietrich, J. Simulation of Irrigation Demand and Control in Catchments—A Review of Methods and Case Studies. *Water Resour. Res.* **2021**, *57*, 21. [CrossRef]
30. Xiu, H.; Wu, L. Hydrodynamic Research of Flood Routing in the Plain River Network Based on MIKE II. *South-North Water Divers. Water Sci. Technol.* **2012**, *10*, 151–154.
31. Ruiju, L.; Wcnhui, C.; Wenxiang, C.; Xieyao, M. Hydrological system model for Taihu lake drainage basin. *Lake Sci.* **1993**, *5*, 99–107. [CrossRef]
32. Patel, D.P.; Ramirez, J.A.; Srivastava, P.K.; Bray, M.; Han, D.W. Assessment of flood inundation mapping of Surat city by coupled 1D/2D hydrodynamic modeling: A case application of the new HEC-RAS 5. *Nat. Hazards* **2017**, *89*, 93–130. [CrossRef]
33. Chen, G.; Wang, C.H.; Fang, X.; Li, X.N.; Zhang, P.N.; Hua, W.J. Distributed-Framework Basin Modeling System: IV. Application in Taihu Basin. *Water* **2021**, *13*, 611. [CrossRef]
34. Hu, Z.J.; Wang, L.L.; Tang, H.W.; Qi, X.M. Prediction of the future flood severity in plain river network region based on numerical model: A case study. *J. Hydrodyn.* **2017**, *29*, 586–595. [CrossRef]
35. Shikasho, S.; Tanaka, K. Runoff Analysis of Low-Lying Drainage Basins in Japan. *J. Irrig. Eng. Rural Plan.* **1985**, *1985*, 5–17. [CrossRef]
36. Chen, R.S.; Pi, L.C. Application of diffusive tank model in drainage analysis of paddy fields. *J. Am. Water Resour. Assoc.* **2004**, *40*, 33–41. [CrossRef]
37. Xiong, Y.; Liu, Z.; Liu, F.; Yuan, N.; Fu, H. The Waterlogging Process Model in the Paddy Fields of Flat Irrigation Districts. *Water* **2021**, *13*, 2668. [CrossRef]
38. Sampson, J.R. Adaptation in natural and artificial systems (John H. Holland). *SIAM Rev.* **1976**, *18*, 529–530. [CrossRef]
39. Liu, Z.; Xiong, Y.; Xu, J.; Yang, S.; Jiang, Z.; Liu, F. Optimal Operation Model of Drainage Works for Minimizing Waterlogging Loss in Paddy Fields. *Water* **2021**, *13*, 2811. [CrossRef]
40. Zeng, L.H.; Lesch, S.M.; Grieve, C.M. Rice growth and yield respond to changes in water depth and salinity stress. *Agric. Water Manag.* **2003**, *59*, 67–75. [CrossRef]
41. Liu, Z.; Xiong, Y.; Fan, L.; Xu, J. Waterlogging Loss Evaluation Model for Waterlogging Process at Flat Irrigation District. *Water Sav. Irrig.* **2021**, *11*, 20–24. [CrossRef]
42. Moriasi, D.N.; Arnold, J.G.; Van Liew, M.W.; Bingner, R.L.; Harmel, R.D.; Veith, T.L. Model evaluation guidelines for systematic quantification of accuracy in watershed simulations. *Trans. ASABE* **2007**, *50*, 885–900. [CrossRef]
43. Schaefli, B.; Gupta, H.V. Do Nash values have value? *Hydrol. Process.* **2007**, *21*, 2075–2080. [CrossRef]
44. Xiong, Y.; Xu, J.; Li, Y.; Li, J.a.; Sun, Y. Modeling waterlogging process of paddy field at flat irrigation district in south China. *J. Drain. Irrig. Mach. Eng.* **2018**, *36*, 725–731.
45. Yan, D.H.; Wu, D.; Huang, R.; Wang, L.N.; Yang, G.Y. Drought evolution characteristics and precipitation intensity changes during alternating dry-wet changes in the Huang-Huai-Hai River basin. *Hydrol. Earth Syst. Sci.* **2013**, *17*, 2859–2871. [CrossRef]
46. Gu, X.Z.; Ye, L.; Xin, Q.; Zhang, C.; Zeng, F.Z.; Nerantzaki, S.D.; Papalexiou, S.M. Extreme Precipitation in China: A Review on Statistical Methods and Applications. *Adv. Water Resour.* **2022**, *163*, 20. [CrossRef]
47. *SL 44-2006*; Regulation for Calculating Design Flood of Water Resources and Hydropower Projects. Ministry of Water Resources of the People's Republic of China: Beijing, China, 2006.
48. Wen, X.; Fang, G.H.; Qi, H.S.; Zhou, L.; Gao, Y.Q. Changes of temperature and precipitation extremes in China: Past and future. *Theor. Appl. Climatol.* **2016**, *126*, 369–383. [CrossRef]

49. Yuan, Z.; Yang, Z.Y.; Yan, D.H.; Yin, J. Historical changes and future projection of extreme precipitation in China. *Theor. Appl. Climatol.* **2017**, *127*, 393–407. [CrossRef]
50. Xu, J.Z.; Peng, S.Z.; Yang, S.H.; Wang, W.G. Ammonia volatilization losses from a rice paddy with different irrigation and nitrogen managements. *Agric. Water Manag.* **2012**, *104*, 184–192. [CrossRef]
51. Shao, C.; Pan, X.; Li, J.; Wei, P.; Zhang, X.; Hu, Q.; Ren, J. Effects of flooding duration in different growth stages on growth and yield component of rice. *Trans. Chin. Soc. Agric. Eng.* **2019**, *35*, 125–133.
52. Wu, Q.; Yang, W.; Zhu, J.; Wang, Z.; Ye, H. Response of hybrid rice to flooding and establishment of drainage index. *Resour. Environ. Yangtze Basin* **2014**, *23*, 875–882.